Mutations in CSPP1 cause primary cilia abnormalities and Joubert syndrome with or without Jeune asphyxiating thoracic dystrophy

Tuz, Karina ; Bachmann-Gagescu, Ruxandra ; O'Day, Diana R ; Hua, Kiet ; Isabella, Christine R ; Phelps, Ian G ; Stolarski, Allan E ; O'Roak, Brian J ; Dempsey, Jennifer C ; Lourenco, Charles ; Alswaid, Abdulrahman ; Bönnemann, Carsten G ; Medne, Livija ; Nampoothiri, Sheela ; Stark, Zornitza ; Leventer, Richard J ; Topçu, Meral ; Cansu, Ali ; Jagadeesh, Sujatha ; Done, Stephen ; Ishak, Gisele E ; Glass, Ian A ; Shendure, Jay ; Neuhauss, Stephan C F ; Haldeman-Englert, Chad R ; Doherty, Dan ; Ferland, Russell J

Abstract: Joubert syndrome (JBTS) is a recessive ciliopathy in which a subset of affected individuals also have the skeletal dysplasia Jeune asphyxiating thoracic dystrophy (JATD). Here, we have identified biallelic truncating CSPP1 (centrosome and spindle pole associated protein 1) mutations in 19 JBTS-affected individuals, four of whom also have features of JATD. CSPP1 mutations explain 5% of JBTS in our cohort, and despite truncating mutations in all affected individuals, the range of phenotypic severity is broad. Morpholino knockdown of cspp1 in zebrafish caused phenotypes reported in other zebrafish models of JBTS (curved body shape, pronephric cysts, and cerebellar abnormalities) and reduced ciliary localization of Arl13b, further supporting loss of CSPP1 function as a cause of JBTS. Fibroblasts from affected individuals with CSPP1 mutations showed reduced numbers of primary cilia and/or short primary cilia, as well as reduced axonemal localization of ciliary proteins ARL13B and adenylyl cyclase III. In summary, CSPP1 mutations are a major cause of the Joubert-Jeune phenotype in humans; however, the mechanism by which these mutations lead to both JBTS and JATD remains unknown.

DOI: https://doi.org/10.1016/j.ajhg.2013.11.019

ARTICLE

Mutations in *CSPP1* Cause Primary Cilia Abnormalities and Joubert Syndrome with or without Jeune Asphyxiating Thoracic Dystrophy

Karina Tuz,[1,21] Ruxandra Bachmann-Gagescu,[2,3,21] Diana R. O'Day,[4,21] Kiet Hua,[1] Christine R. Isabella,[4] Ian G. Phelps,[4] Allan E. Stolarski,[1] Brian J. O'Roak,[5] Jennifer C. Dempsey,[4] Charles Lourenco,[6] Abdulrahman Alswaid,[7] Carsten G. Bönnemann,[8] Livija Medne,[9] Sheela Nampoothiri,[10] Zornitza Stark,[11] Richard J. Leventer,[12] Meral Topçu,[13] Ali Cansu,[14] Sujatha Jagadeesh,[15] Stephen Done,[16] Gisele E. Ishak,[16] Ian A. Glass,[4,17] Jay Shendure,[18] Stephan C.F. Neuhauss,[2] Chad R. Haldeman-Englert,[19] Dan Doherty,[4,17,*] and Russell J. Ferland[1,20,*]

Joubert syndrome (JBTS) is a recessive ciliopathy in which a subset of affected individuals also have the skeletal dysplasia Jeune asphyxiating thoracic dystrophy (JATD). Here, we have identified biallelic truncating *CSPP1* (centrosome and spindle pole associated protein 1) mutations in 19 JBTS-affected individuals, four of whom also have features of JATD. *CSPP1* mutations explain ~5% of JBTS in our cohort, and despite truncating mutations in all affected individuals, the range of phenotypic severity is broad. Morpholino knockdown of *cspp1* in zebrafish caused phenotypes reported in other zebrafish models of JBTS (curved body shape, pronephric cysts, and cerebellar abnormalities) and reduced ciliary localization of Arl13b, further supporting loss of CSPP1 function as a cause of JBTS. Fibroblasts from affected individuals with *CSPP1* mutations showed reduced numbers of primary cilia and/or short primary cilia, as well as reduced axonemal localization of ciliary proteins ARL13B and adenylyl cyclase III. In summary, *CSPP1* mutations are a major cause of the Joubert-Jeune phenotype in humans; however, the mechanism by which these mutations lead to both JBTS and JATD remains unknown.

Introduction

Joubert syndrome (JBTS [MIM 213300]) is a recessive developmental disorder characterized by congenital hindbrain malformations including cerebellar vermis hypoplasia, thick superior cerebellar peduncles, a deep interpeduncular fossa, and a variety of other brain-imaging abnormalities.[1–4] Individuals with JBTS have ataxia, hypotonia, cognitive impairment, and abnormal breathing and eye movements.[1–3] In addition, subsets of individuals with JBTS have retinal dystrophy, nephronophthisis, hepatic fibrosis, and polydactyly. JBTS is one of an expanding group of disorders known as ciliopathies, unified by their overlapping clinical features and shared pathologic mechanisms involving the primary cilium.[5] Mutations in at least 20 genes can cause JBTS; however, the genetic cause remains unidentified in approximately half of individuals with JBTS.

Jeune asphyxiating thoracic dystrophy (JATD [MIM 208500]) is another autosomal-recessive ciliopathy[6] and principally affects cartilage and bone development.[7–11] Individuals with JATD are characterized primarily by having smaller and narrower rib cages, which often lead to respiratory failure and death as a result of an inability to fully expand the lungs.[11] Affected individuals who survive often develop cystic kidney and liver disease.[12] Although mutations in five genes have been shown to cause JATD,[7–10,13] details of the mechanisms underlying JATD remain unknown.

Previously, we reported on four individuals with co-occurring JBTS and JATD, possibly representing a genetically distinct ciliopathy phenotype.[14] Here, we identify a genetic cause of JBTS that accounts for half of our families affected by co-occurring JATD, and we demonstrate defects in primary cilia in cell lines from affected individuals, as well as ciliopathy phenotypes in a zebrafish model.

[1]Center for Neuropharmacology and Neuroscience, Albany Medical College, Albany, NY 12208, USA; [2]Institute of Molecular Life Sciences, University of Zurich, 8057 Zurich, Switzerland; [3]Institute of Medical Genetics, University of Zurich, 8603 Zurich, Switzerland; [4]Divisions of Genetic Medicine and Developmental Medicine, Department of Pediatrics, University of Washington, Seattle, WA 98195, USA; [5]Department of Molecular & Medical Genetics, Oregon Health Sciences University, Portland, OR 97239, USA; [6]Neurogenetics Division, Clinics Hospital, School of Medicine of Ribeirão Preto, University of São Paulo, Ribeirão Preto, São Paulo 14049-900, Brazil; [7]Department of Pediatrics, King Abdulaziz Medical City, Riyadh 11426, Saudi Arabia; [8]Neuromuscular and Neurogenetic Disorders of Childhood Section, John Edward Porter Neuroscience Research Center, National Institutes of Health, Bethesda, MD 20892, USA; [9]Division of Neurology, Children's Hospital of Philadelphia, Philadelphia, PA 19104, USA; [10]Department of Pediatric Genetics, Amrita Institute of Medical Sciences and Research Center, AIMS Ponekkara Post Office, Kochi, Kerala 682041, India; [11]Victorian Clinical Genetics Services, Murdoch Childrens Research Institute, Parkville, VIC 3052, Australia; [12]Departments of Neurology and Pediatrics, Murdoch Childrens Research Institute, Royal Children's Hospital and University of Melbourne, Parkville, VIC 3052, Australia; [13]Department of Child Neurology, Hacettepe University Medical Faculty, Ihsan Dogramacı Children's Hospital, Ankara 06100, Turkey; [14]Pediatric Neurology Unit, De Karadeniz Technical University, Trabzon 61080, Turkey; [15]MediScan Systems, Mylapore, Chennai 600 004, India; [16]Department of Radiology, University of Washington and Seattle Children's Hospital, Seattle, WA 98105, USA; [17]Center for Integrative Brain Research, Seattle Children's Hospital Research Institute, Seattle, WA 98105, USA; [18]Department of Genome Sciences, University of Washington, Seattle, WA 98195, USA; [19]Department of Pediatrics, Section on Medical Genetics, Wake Forest School of Medicine, Winston-Salem, NC 27157, USA; [20]Department of Neurology, Albany Medical College, Albany, NY 12208, USA
[21]These authors contributed equally to this work
*Correspondence: ddoher@uw.edu (D.D.), ferlanr@mail.amc.edu (R.J.F.)
http://dx.doi.org/10.1016/j.ajhg.2013.11.019.

Subjects and Methods

Study Participants

Inclusion criteria for participants were (1) molar tooth sign on brain imaging (or cerebellar vermis hypoplasia on computed-tomography [CT] scan when MRI was not available) and (2) clinical findings of JBTS (hypotonia, ataxia, oculomotor abnormalities, cognitive impairment, and/or abnormal respiratory control). All available MRI or CT scans of affected individuals were read by multiple neurologists, and JBTS was diagnosed according to accepted diagnostic criteria. Genomic DNA and/or skin biopsies were obtained with informed consent from all participating study subjects. The study was reviewed and approved by the institutional review boards at Albany Medical College and the University of Washington.

Exon Capture and Sequencing

Molecular inversion probes (MIPs) captured all coding exons and 10 bp of exon-flanking intronic sequence in centrosome and spindle pole associated protein 1 (*CSPP1* [MIM 611654, RefSeq accession number NM_024790.6]). MIP design and library preparation were performed as described previously.[15] In summary, pooled MIPs captured *CSPP1* exons from 100 ng of DNA per sample. Captures were PCR amplified with universal primers, and each reverse primer contained a unique 8-base barcode. After amplification, barcoded libraries were pooled and multiplex sequenced with 101-cycle, paired-end reads on the Illumina HiSeq platform.

Variant Identification

Raw sequence reads were processed and aligned to the hg19 human reference sequence (UCSC Genome Browser) with the Burrows-Wheeler Aligner (BWA, version 0.5.9)[16] as described.[15] BAM files were generated with Picard tools (see Web Resources), and single-nucleotide variants (SNVs) and indels were called with the Genome Analysis Toolkit (GATK, see Web Resources) UnifiedGenotyper,[17] in which the dcov parameter was set to 5,000. GATK was used for filtering variants according to the following metrics: allele balance > 0.8, quality < 30, read depth $< 25\times$, quality by depth < 5, and a window of 10 for clustered variants. Variants were annotated with SeattleSeq (see Web Resources) and further filtered against controls from the National Heart, Lung, and Blood Institute (NHLBI) Exome Sequencing Project Exome Variant Server (EVS) ESP6500 data set (see Web Resources) with the use of an observed mean allele frequency threshold $< 1\%$. Of the variants meeting these criteria, only nonsense, nonsynonymous, frameshift, and splice-site variants were considered for further analysis. The GATK DepthOfCoverage tool was used for determining *CSPP1* sequence coverage. Positions with read depths $\geq 25\times$ were considered covered. Confirmation and segregation of identified *CSPP1* variants were performed by Sanger sequencing for all family members when DNA was available.

Zebrafish Studies

Zebrafish (*Danio rerio*) were maintained as previously described.[18] Embryos were raised at 28°C. All zebrafish protocols used in the research described in this work were in compliance with internationally recognized guidelines for the use of fish in biomedical research, and the experiments were approved by local authorities (Veterinäramt Zürich TV4206).

Morpholino oligonucleotides *cspp1a* ex2i2 5′-ATTGAAATATAG CCTGCCTTTGGTC-3′, ex22i22 5′-AGAGTTGAGTGTCAGACT TACCTCT-3′, and *cspp1b* ex2i2 5′-TGCAAACAGAACTCTAC CTTGCTGA-3′ (Gene Tools, LLC) were injected into zebrafish embryos at the 1- to 2-cell stage.

Whole-mount antibody staining was performed on zebrafish embryos fixed with 4% paraformaldehyde (PFA) according to standard protocols. Primary antibodies were rabbit polyclonal anti-arl13b (1:100, gift from Z. Sun, Yale University)[19] and mouse monoclonal anti-acetylated α-tubulin (1:500, Sigma). Secondary antibodies were Alexafluor goat anti-rabbit or goat anti-mouse IgG (Life Technologies) used at 1:300. Images were acquired on a Leica HCS LSI confocal microscope with identical settings for morphant and control fish. Fluorescence intensities were measured on single confocal sections with ImageJ,[20] which was blinded to injection status. In situ hybridizations on zebrafish embryos were performed according to standard protocols. In situ probes against *cspp1a* were generated with primers 5′-ATTGGAGG GACAGTTAATACAG-3′ and 5′-AGGAACTGGCTCGTAACC-3′. Zebrafish cartilage staining with Alcian Blue was performed according to standard protocols.[21]

Cell Culture

Human dermal fibroblasts were collected from JBTS-affected individuals with *CSPP1* mutations and from noncarrier siblings through skin-punch biopsies after informed consent was obtained. Tissue was treated with collagenase and cultured in Dulbecco's modified Eagle's medium (DMEM) supplemented with 10% fetal bovine serum (FBS), 1% penicillin, and 1% streptomycin. Once the cultures were confluent, the cells were trypsinized (0.05% in EDTA) for 5 min at 37°C, and trypsin was subsequently inactivated with culture media containing 10% FBS. Cell suspensions were plated on cell-culture plates or glass coverslips (treated with 0.1% gelatin) and maintained at 37°C in a humidified atmosphere (5% CO_2 and 95% air). For promoting robust cilia formation, fibroblast cultures were starved in DMEM containing 0.1% FBS for 48 hr.

Immunostaining and Microscopy

Human dermal fibroblasts grown on coverslips were fixed with cold methanol (−20°C), 4% PFA in PBS, or 2% PFA in microtubule-stabilizing buffer. Cell cultures were washed with PBS and permeabilized with 0.04% Triton X-100 in PBS (PBS-Tx) and blocked with 10% normal goat serum in PBS-Tx for 1 hr at room temperature. Primary antibodies were incubated overnight at 4°C and diluted in 1% normal goat serum in PBS-Tx as follows: rabbit polyclonal anti-CSPP1, 1:200 (Proteintech); mouse monoclonal anti-γ-tubulin, 1:1,000 (Sigma); mouse monoclonal anti-acetylated α-tubulin, 1:1,000 (Sigma); rabbit polyclonal anti-adenylyl cyclase III (anti-AC3), 1:200 (Santa Cruz Biotechnology); mouse monoclonal anti-Arl13b, 1:500 (UC Davis/NIH NeuroMab Facility); and rabbit monoclonal anti-Ki-67, 1:500 (Epitomics). Alexafluor secondary antibodies (1:500, Life Technologies) were incubated for 1 hr at room temperature, and Hoechst DNA staining (1 μg/ml) followed. Coverslips were mounted with Fluoromount-G (anti-fade) solution (Southern Biotech). Images were obtained with a Zeiss AxioImager-Z1 microscope equipped with an AxioCam MRm camera and processed with AxioVision Rel. 4.5 software and Adobe Photoshop CS6 (Adobe Systems). For measuring the fluorescence-density differences of ARL13B and AC3 in the primary cilium, all images were taken with the same exposure time. We calculated fluorescence-density differences by outlining each ciliary axoneme and obtaining the area of each

cilium and the raw integrated densities of ARL13B and AC3 immunofluorescence by using these features in ImageJ.[20] We calculated fluorescence density by dividing the raw integrated densities by the ciliary area. Importantly, this approach took into account the area of each cilium.

Immunoblotting

Cells were lysed in Tris lysis buffer (50 mM Tris [pH 8.0], 150 mM NaCl, 1% NP40, 1 mM DTT, 1 mM PMSF, 1 mM EDTA and a protease inhibitor cocktail [Roche]), incubated on ice for 30 min, and centrifuged at 10,000 × *g* for 30 min at 4°C. Protein samples were separated by 8% SDS-PAGE and electroblotted onto a polyvinylidene fluoride membrane. Blots were blocked with 5% nonfat dried milk in TBS-Tx (10 mM Tris, 150 mM NaCl, 0.01% Triton X-100, pH 7.5) for 1 hr at room temperature and incubated overnight with anti-CSPP1 (1:200, Proteintech) at 4° C. Horseradish-peroxidase-conjugated secondary antibodies were detected with the SuperSignal West Femto Maximum Sensitivity Substrate (Thermo Scientific). Chemiluminescence signals were detected and acquired with a G:Box iChemi XT imager system and GeneSnap software (SynGene). Images were processed with the GeneTools software package (SynGene).

mRNA Quantification by RT-PCR

RNA from human dermal fibroblast cultures was extracted with the Ambion RNAqueous-4PCR Kit (Life Technologies), and cDNA was synthesized with qScript cDNA SuperMix (Quanta Biosciences). PCR primers were designed against the 5′ end (forward primer 5′-GTGGCCGCTGTAACCTCTT-3′ and reverse primer 5′-TCAGAAAGCTTCGCTGACAA-3′) and the 3′ end (forward primer 5′-CTGCCAGGAAAAATCAGCTC-3′ and reverse primer 5′-GCC CTTAGGGGACTGTCTTC-3′) of *CSPP1* for amplifying ~200 bp fragments. PCR products were separated by agarose gel electrophoresis and stained by ethidium bromide. The intensity of the bands was quantified by densitometry with the GeneTools software (SynGene).

Statistical Analyses

Two-tailed Student's t tests were used for determining statistical significance, except for the number of ciliated cells between groups, for which the nonparametric Mann-Whitney U test was employed. Statistical analyses were performed with Statistica (StatSoft).

Results

CSPP1 Mutations Cause JBTS

A single region of copy-number-neutral absence of heterozygosity was identified by a clinical SNP microarray (Affymetrix SNP 6.0) in chromosomal region 8q13.1–q21.12 in a male newborn (JS-1701) born to nonconsanguineous parents and with a primary diagnosis of JBTS. The region encompasses 40 genes present in OMIM (Table S1, available online), and Sanger sequencing identified a homozygous nonsense mutation (c.2320C>T [p.Arg774*]) in *CSPP1* (Figure 1 and Table 1). This mutation is not present in 11,906 chromosomes in the NHLBI EVS data set of 6,500 exomes (see Web Resources). To validate loss of *CSPP1* function as a cause of JBTS, we sequenced all coding exons of *CSPP1* plus 10 bp of flanking intronic sequence in a cohort of 384 affected individuals from 320 families by using a highly efficient targeted-sequencing method.[15] Individuals with known genetic causes of JBTS were not excluded from the cohort, and of note, eight affected individuals in six families had JBTS and features of JATD.

Eighteen individuals from 14 families were shown to carry biallelic mutations in *CSPP1*, accounting for ~5% of the families in our cohort (Figure 1A and Table 1). All of the mutations are rare (<0.03%) in the NHLBI EVS data set and are predicted to truncate the protein (nonsense, frameshift, splice site); one such mutation of the last base pair in exon 9 (in family UW141) results in aberrant splicing. *CSPP1* mRNA from UW141-3 fibroblasts has 10 bp inserted into the transcript, creating a stop codon immediately downstream of the disrupted splice site (Figure S1). When DNA samples were available from family members, we confirmed by Sanger sequencing that the variants segregated appropriately for autosomal-recessive inheritance. We identified rare biallelic missense variants in three samples; however, in two cases, the missense variants did not segregate appropriately for autosomal-recessive inheritance, and in the third, the affected individual had a homozygous frameshift mutation (c.7988_7989delGA [p.Gly2663Alafs*40]) in *C5ORF42* (MIM 614571, RefSeq NM_023073.3). Three families from Brazil (UW123, UW124, and UW148), not known to be related, shared the same two *CSPP1* mutations (c.3211_3212insA [p.Tyr1071*] and c.2953+1G>A [splice]), suggesting that these families are, in fact, related. In addition, c.2527_2528delAT (p.Met843Glufs*25) was shared by one Lebanese and two Turkish families, indicating that it is most likely a founder mutation.

Broad Phenotype in Humans

We were able to collect detailed clinical information for 18 of the 19 affected individuals, revealing a very broad spectrum of phenotypic severity (Table 1). The most severely affected individuals showed profound developmental disability (n = 7), occipital encephalocele (n = 1), cleft palate (n = 1), and/or skeletal features compatible with JATD (n = 3 families, 4 affected individuals; Figure 1B and Table 1), for which two received mechanical ventilation. Two siblings (UW129-3 and UW129-4) showed evidence of liver fibrosis and chronic sinusitis without pulmonary issues. Two other unrelated affected individuals had retinal dystrophy, and another had echogenic kidneys, but none had coloboma or polydactyly. Affected individuals at the mild end of the spectrum had mild developmental disability, no retinal, renal, or liver involvement, and no features of JATD. We observed no obvious correlation between the position of the truncating mutations and the phenotype, and in fact, the least severely affected individuals had the most N-terminal truncating mutations.

The brain MRI findings in ten individuals also displayed a wide range of severity (Table S2). In addition to the

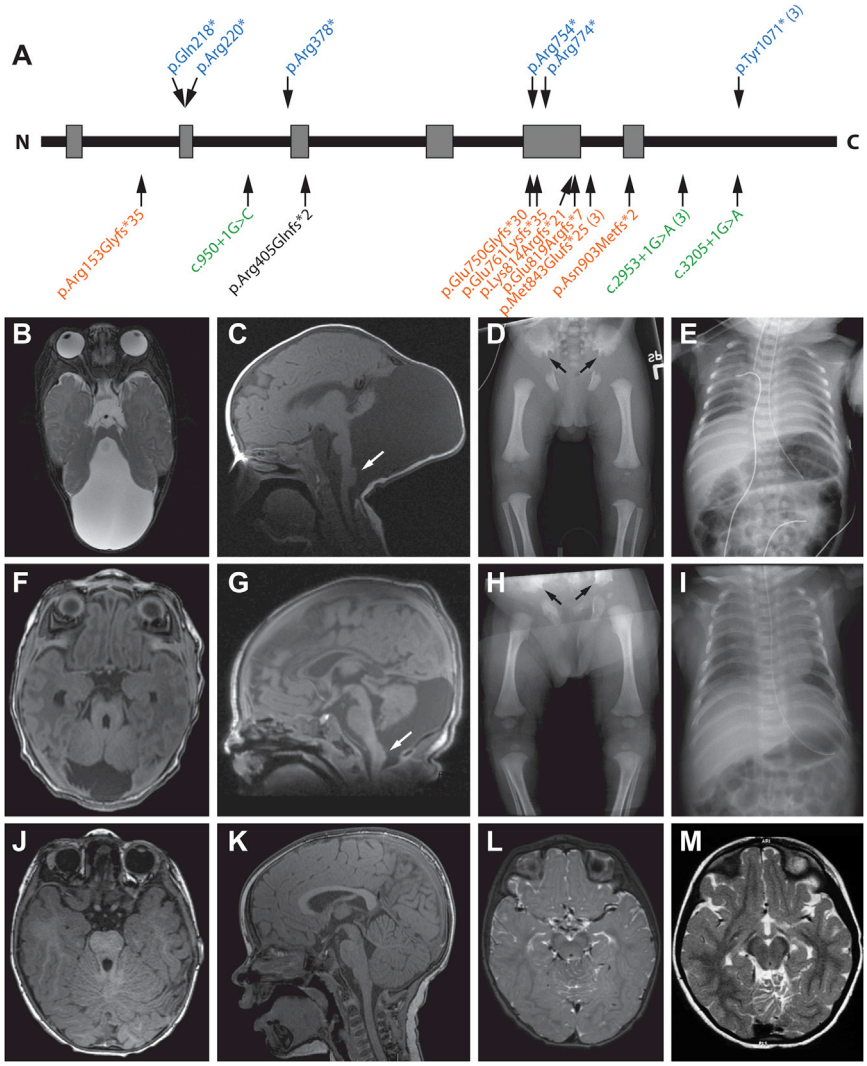

Figure 1. Spectrum of Brain- and Skeletal-Imaging Findings in Individuals with *CSPP1*-Related JBTS

(A) CSPP1 schematic showing the coiled-coil domains (gray rectangles). Nonsense truncating variants (blue) are indicated above the protein at their approximate locations. Frameshift truncating variants (orange), variants affecting canonical splice sites (green), and a missense variant (a coding variant that results in a frameshift because of aberrant splicing; black; see Figure S1) are indicated below the protein. The number of times a specific variant was identified in the cohort is indicated in parentheses after the variant.

(B–E) Molar tooth sign (B), cervicomedullary heterotopia (white arrow) and occipital encephalocele (C), trident acetabulae with inferolateral spurs (black arrows) and mildly short femurs (D), and a mildly narrow chest with horizontal ribs (E) in JS-1701.

(F–I) Molar tooth sign (F), cervicomedullary heterotopia (white arrow) and retrocerebellar fluid collection (G), trident acetabulae with inferolateral spurs (black arrows in H), and a narrow chest with horizontal ribs (I) in UW147-3.

(J–L) Normal superior cerebellar peduncles (J), mild cerebellar vermis hypoplasia (K), and superior cerebellar dysplasia (L) in UW141-4.

(M) Superior vermis dysplasia in UW151-3, who has a classic molar tooth sign (not shown).

(B), (L), and (M) are T2-weighted images. (C), (F), (G), (J), and (K) are T1-weighted images.

individual with the large occipital encephalocele, five of ten had a posterior gap in their foramen magnum, presumably the mildest form of occipital encephalocele in JBTS. Multiple affected individuals had cortical (three of ten), midbrain (six of ten), and cervicomedullary (four of ten) heterotopia. Of note, UW141-4 had a subset of the imaging findings typically seen in individuals with JBTS (Figures 1J–1L): mild cerebellar vermis hypoplasia (Figure 1K) and superior cerebellar dysplasia (compare Figure 1L to Figure 1M) without thick, misoriented superior cerebellar peduncles (Figures 1J and 1K). Unfortunately, MRI for his brother was not available for review; however, both brothers had hypotonia, ataxia, and oculomotor apraxia, and UW141-3 had tachypnea as an infant, strongly supporting a JBTS diagnosis.

cspp1 Knockdown in Zebrafish Recapitulates Ciliopathy Phenotypes

To investigate the function of *CSPP1*, we examined the effects of *cspp1* knockdown in zebrafish. Zebrafish have two putative orthologs for *CSPP1*, one on chromosome 24 (*cspp1a*) and a second on chromosome 2 (*cspp1b*). Given that the conservation is higher for *cspp1a* than for *cspp1b*, which also encodes a shorter protein, we initially focused on *cspp1a*. Using in situ hybridization, we determined that *cspp1a* was strongly expressed ubiquitously at 24 hr postfertilization (hpf), including in the brain and ear (Figures S2A and S2A′). At 48 hpf, expression decreased globally but remained high in the cerebellar fold, ear, and nose pits and became detectable in the fin buds and somites and ventrally just above the yolk (Figures S2B and S2C).

Two different splice morpholinos were used for knocking down *cspp1a* function—(1) MOe2i2, targeting the exon-intron boundary after exon 2 and expected to cause retention of intron 2 and lead to a stop codon just after exon 2, and (2) MOex22i22, targeting the exon-intron boundary after exon 22—and for modeling the human splice mutation identified in families UW123, UW124, and UW148. The morpholinos efficiently disrupted normal splicing in *cspp1a* morphants at 2 days postfertilization (dpf) (Figures S2D and S2D′). Knockdown of *cspp1a* with either of the morpholinos led to a curved body shape, dilated ventricles, and pronephric cysts, a combination of

Table 1. Clinical Phenotypes of Individuals with *CSPP1*-Related JBTS

Individual	cDNA[a] Mutation (Allele)	Protein Alteration	Ethnicity	Age	Seizures	Abnormal Respiratory Pattern	Abnormal Eye Movements	Retina	Kidney	Ptosis	Encephalocele	Other
JS-1701	homozygous c.2320C>T	homozygous p.Arg774*	African American	1 year	N	A	N	N	N	Y	Y	JATD, MV, hypertelorism, NG tube, megalopapillae, optic atrophy
UW035-3	homozygous c.2708delA (P, M)	homozygous p.Asn903Metfs*2	Saudi Arabian	12 years	Y	T	nystagmus	N	N	Y	N	-
UW097-3	c.2244_2245delAA (P)	p.Glu750Glyfs*30	mixed European	4 years	N	A or T	nystagmus, OMA	Y	N	Y	N	JATD, G-tube, third-nerve palsy
	c.2280delA (M)	p.Glu761Lysfs*35										
UW097-6	c.2244_2245delAA (P)	p.Glu750Glyfs*30	mixed European	4 months	N	A or T	nystagmus	N	Y[b]	Y	N	JATD, MV, G-tube, dysphagia
	c.2280delA (M)	p.Glu761Lysfs*35										
UW123-3	c.3211_3212insA (P)	p.Tyr1071*	Brazilian	10 years	N	A or T	nystagmus	N	N	Y	N	-
	c.2953+1G>A (M)	splice										
UW124-3	c.3211_3212insA (P)	p.Tyr1071*	Brazilian	14 years	N	A or T	nystagmus	N	N	Y	N	-
	c.2953+1G>A (M)	splice										
UW127-3	homozygous c.2448_2454dupAGAAGAA	homozygous p.Glu819Argfs*7	Turkish	unk	unk	unk	unk	unk	unk	unk	unk	-
UW128-3	c.457delA (M)	p.Arg153Glyfs*35	Chinese	2 years	N	T	N	N	N	Y	N	HL
	c.2260C>T (P)	p.Arg754*										
UW129-3	c.658C>T (P)	p.Arg220*	Turkish	21 years	N	N	N	N	N	Y	N	liver fibrosis on biopsy, splenomegaly, elevated transaminases, chronic sinusitis
	c.2527_2528delAT (M)	p.Met843Glufs*25										
UW129-4	c.658C>T (P)	p.Arg220*	Turkish	16 years	N	N	N	N	N	Y	N	elevated transaminases, chronic sinusitis
	c.2527_2528delAT (M)	p.Met843Glufs*25										
UW130-3	homozygous c.2527_2528delAT (P, M)	homozygous p.Met843Glufs*25	Turkish	6 years	N	A or T	N	N	N	Y	N	cleft palate,[c] hypertelorism
UW137-3	c.3205+1G>A (M)	splice	mixed European	22 years	N	T	nystagmus	Y	N	Y	N	high-arched palate
	c.950+1G>C (P)	splice										
UW141-3	c.652C>T (M)	p.Gln218*	northern European	16 years	N	T	OMA	N	N	N	N	obese
	c.1214G>A[d] (P)	p.Arg405Glnfs*2										
UW141-4	c.652C>T (M)	p.Gln218*	northern European	9 years	N	N	OMA	N	N	N	N	-
	c.1214G>A[d] (P)	p.Arg405Glnfs*2										
UW143-3	c.1132C>T	p.Arg378*	Indian	5 years	N	T	N	N	unk	Y	N	hypertelorism, CPEO,[e] mild left optic disc pallor
	c.2441_2444delAGAA	p.Lys814Argfs*21										

(*Continued on next page*)

Table 1. *Continued*

Individual	cDNA[a] Mutation (Allele)	Protein Alteration	Ethnicity	Age	Seizures	Abnormal Respiratory Pattern	Abnormal Eye Movements	Retina	Kidney	Ptosis	Encephalocele	Other
UW143-4	c.1132C>T	p.Arg378*	Indian	2 years	N	N	N	N	unk	N	N	hypertelorism, restricted upward gaze[e]
	c.2441_2444delAGAA	p.Lys814Argfs*21										
UW147-3	homozygous c.2527_2528delAT (P, M)	homozygous p.Met843Glufs*25	Lebanese	7 months	N	A or T	N	N	N	Y	N	JATD, NG tube, HL, high-arched palate
UW148-3	c.3211_3212insA	p.Tyr1071*	Brazilian	9 years	N	A or T	OMA	N	N	Y	N	-
	c.2953+1G>A	splice										
UW151-3	homozygous c.2448_2454delAGAAGAA (M)	homozygous p.Glu817Lysfs*17	Indian	6 years	N	N	N	N	N	Y	N	-

Abbreviations are as follows: A, apnea; CPEO, chronic progressive external ophthalmoplegia; G-tube, gastrostomy tube; HL, hearing loss; JATD, Jeune asphyxiating thoracic dystrophy (short ribs, bell-shaped chest, pulmonary hypoplasia, abnormal iliac notches); M, maternal allele; MV, mechanical ventilation; N, feature is absent; NG tube, nasogastric tube; OMA, oculomotor apraxia; P, paternal allele; T, tachypnea; unk, unknown; and Y, feature is present.
[a]RefSeq accession number NM_024790.6.
[b]Echogenic kidneys.
[c]Two deceased siblings with cleft lip and palate, dysmorphism, midline defects, occipital encephalocele.
[d]c.1214G>A causes a cryptic splice site 10 bp 3′ to the usual splice site, resulting in predicted frameshift p.Arg405Glnfs*2 (Figure S1).
[e]Mother has restricted upward gaze.

phenotypes commonly observed in zebrafish ciliopathy gene mutants and morphants (Figures 2A–2F).[19,22] Also common in zebrafish ciliopathy models,[23] abnormalities in retinal photoreceptor outer segments were not observed in *cspp1a* morphants (data not shown).

Given the observed association with skeletal defects in individuals with *CSPP1*-related JBTS, we examined whether skeletal defects were present in *cspp1* morphants. The first skeletal elements to appear in zebrafish larvae are craniofacial cartilages at 3 dpf; these consist of a set of ventral branchial cartilages and a more dorsal neurocranium that lies just ventral to the brain.[24] In both sets of cartilages, knockdown of *cspp1a* consistently caused defects that were not observed in embryos injected with standard control morpholinos (Figures 2G–2H′). Most prominently, the neurocranium showed patterning defects with interruption or absence of the trabeculae, linking the anterior-most neurocranium (ethmoid plate) to the more posterior neurocranium (arrow and arrowhead in Figures 2G and 2G′). On the ventral side, all of the expected skeletal elements were present, but the anterior-posterior length of the branchial cartilages was severely reduced (double-headed arrow in Figures 2H and 2H′).

Knockdown of *cspp1a* in zebrafish did not appear to alter the presence of cilia. Immunofluorescence staining with anti-acetylated α-tubulin and anti-Arl13b showed no effect on the number of cilia in *cspp1a* single morphants or in *cspp1a*+*cspp1b* double morphants (created for excluding the possibility of redundancy with *cspp1b* in ciliogenesis), despite the presence of the above-mentioned phenotypes, including hydrocephalus and pronephric cysts (Figures 2I–2J′ and Figures S2E and S2E′). However, considering the raw integrated fluorescence intensity divided by ciliary area or the ratio of Arl13b fluorescence to acetylated α-tubulin fluorescence for each cilium, we did note that the intensity of Arl13b immunofluorescence in floor-plate cilia was significantly lower in the morphants than in the uninjected or standard-control-morpholino-injected embryos (Figures 2I–2K; average ratio of Arl13b intensity to acetylated α-tubulin intensity was 0.25 in *cspp1* morphants and 1.2 in uninjected embryos, $p < 0.0001$). A role for zebrafish *cspp1a* and/or *cspp1b* in ciliogenesis cannot be entirely excluded by these experiments, given that small amounts of residual protein might still be present because of incomplete activity of the morpholino or the maternal deposition of *cspp1* transcript(s) and/or protein in the egg. Nevertheless, the fact that phenotypes such as pronephric cysts or hydrocephalus were observed in the absence of an obvious ciliogenesis defect indicates that zebrafish *cspp1a* and *cspp1b* are most likely involved in other aspects of ciliary function, including ciliary Arl13b localization.

CSPP1 Is Absent from Ciliary Axonemes in Fibroblasts from Individuals with *CSPP1*-Related JBTS

Previously, CSPP1 has been shown to localize to the basal body and axoneme of primary cilia.[25] In control

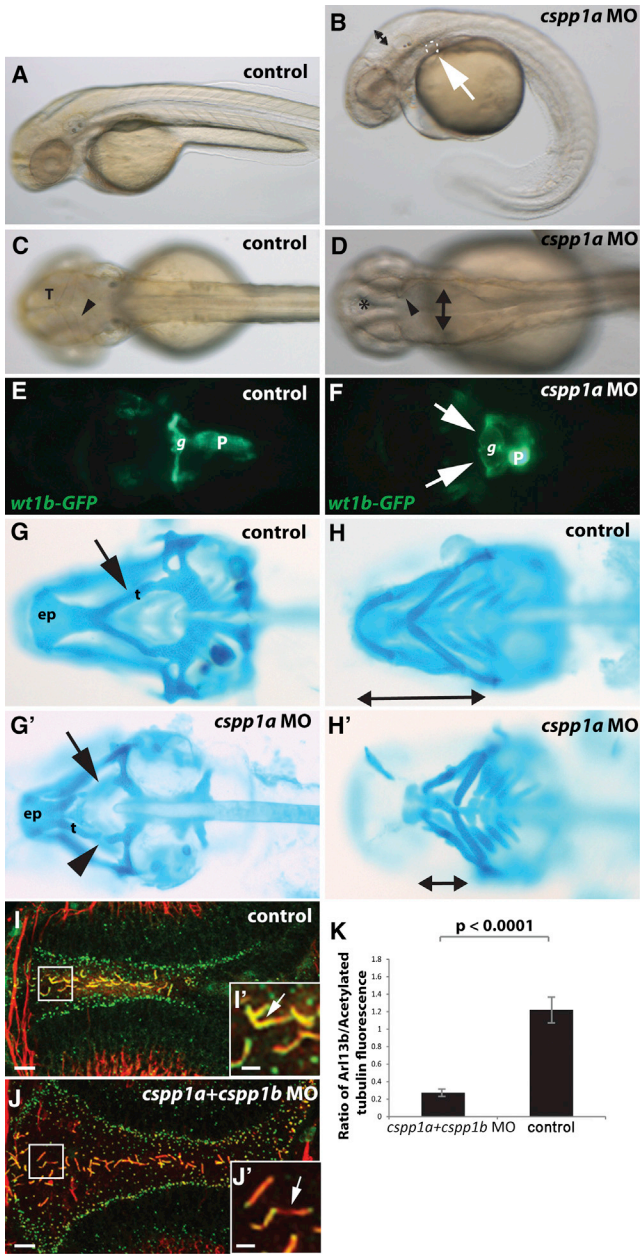

Figure 2. Ciliopathy Phenotypes in *cspp1* Zebrafish Morphants
(A–F) Morpholino knockdown of *cspp1a* resulted in a curved body shape (B) and dilated brain ventricles (double-headed arrows in B and D) associated with an increased gap between the two sides of the tectum (asterisk in D) and a thin cerebellar fold (arrowhead in D, compared to arrowhead in C). Pronephric cysts were observed in *cspp1a* morphants (white arrows in B and F), as highlighted in the *wt1b*-GFP transgenic line (E versus F).
(G–H′) Knockdown of *cspp1a* also led to abnormal development of head cartilages, affecting both the neurocranium (G and G′) and the branchial cartilages (H and H′). Observed phenotypes included interruption (arrowhead in G′) or loss (arrow in G′) of trabeculae and shortened distance between the branchial cartilages (double arrow in H′). The wild-type is shown in (H) for comparison.
(I and J) Immunolabeling of floor-plate cilia in 48 hpf uninjected (I) and *cspp1a*+*cspp1b* double-morpholino-injected embryos (J) with anti-Arl13b (green) and anti-acetylated α-tubulin (red) shows decreased Arl13b fluorescence (arrows in I′ and J′).
(K) The ratio of Arl13b fluorescence to acetylated α-tubulin fluorescence was significantly lower in *cspp1a*+*cspp1b* double morphants than in uninjected embryos ($p < 0.0001$, n = 20 morphants and 15 uninjected embryos). Results are expressed as the mean ± SEM. Abbreviations are as follows: p, pancreas; g, glomerulus; T, tectum; t, trabeculae; and ep, ethmoid plate. The anterior is to the left in all panels. Embryo ages are 48 hpf (A–D), 3 dpf (E and F), 6 dpf (G and H), and 48 hpf (I and J). Scale bars represent 10 μm (I and J) and 5 μm (I′ and J′).

fibroblasts, the previously validated anti-CSPP1, generated against the N terminus (amino acids 1–208),[25] labels both the basal body and the primary cilium (marked with γ-tubulin and acetylated α-tubulin, respectively; Figures 3A and 3B). In fibroblasts from JBTS-affected individuals, UW097-3 and UW141-3, no CSPP1 signal was present in the axoneme, whereas the signal at the base of the cilium remained (Figures 3A and 3B), suggesting that truncated CSPP1 might have been present. To test whether *CSPP1* nonsense-mediated decay was incomplete, we performed RT-PCR, demonstrating that *CSPP1* mRNA expression was reduced by more than 50% in both affected fibroblast lines (Figure S3A). On immunoblots, the N-terminal anti-CSPP1 detected full-length CSPP1 in unaffected fibroblasts, but not in affected cells (Figure S3B); truncated CSPP1 was below the level of detection in affected fibroblasts (data not shown), most likely as a result of, at least in part, the reduction in mRNA expression. Nonetheless, it is clear that CSPP1 localization at the ciliary axoneme is absent in affected cell lines.

Cilium Defects in Fibroblasts from Individuals with *CSPP1*-Related JBTS

Given that CSPP1 localizes to primary cilia and that small interfering RNA knockdown of *CSPP1* has been shown to decrease the number of ciliated hTERT-immortalized retinal pigment epithelial (hTERT-RPE)[25] and human-derived retinal pigment epithelial cells (data not shown), we evaluated whether *CSPP1* mutations are associated with cilia defects by using acetylated α-tubulin and ARL13B immunolabeling to quantify the number and length of primary cilia in unaffected and affected cell lines. To induce robust cilia formation in the fibroblast cell lines, we serum starved the cultures for 48 hr. Using both ciliary axoneme markers, we observed a significant reduction in cilium number in one of the affected cell lines, UW141-3 (Figures 4A and 4C–4E); however, cilium length was decreased in both affected fibroblast lines in that it measured approximately half the cilium length in control fibroblasts (Figures 4A, 4B, and 4D). To determine whether UW141-3 fibroblasts made fewer cilia because they were not able to enter G_0, we immunostained each of the cell lines with anti-Ki-67, a marker expressed in cycling cells. Only a small percentage of serum-starved cells (6%–10%) expressed Ki-67, and no differences were noted between unaffected and affected cells (Figures S4A and S4B).

Many of the proteins implicated in JBTS function at the transition zone of the proximal cilium to regulate protein traffic in and out of the cilium.[26–30] Given that loss of

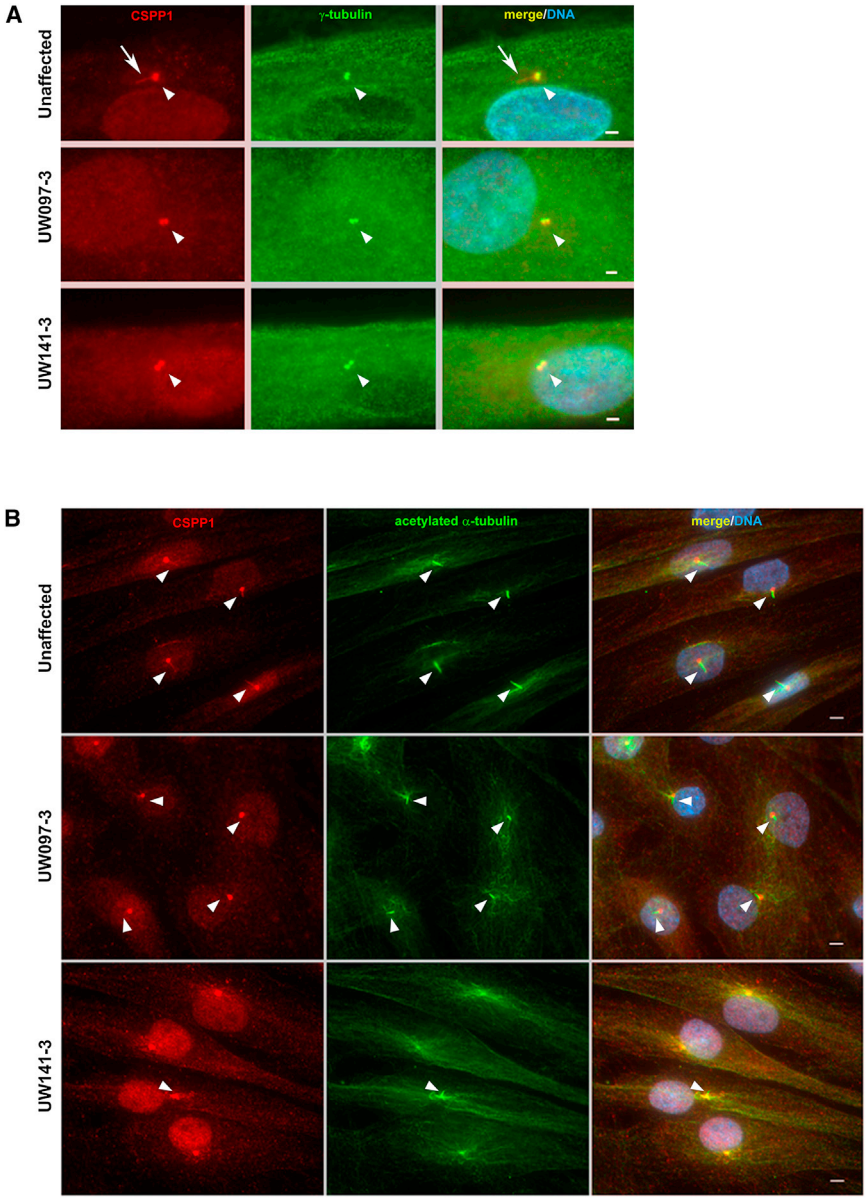

Figure 3. CSPP1 Is Not Localized in the Primary Cilia Axoneme of Dermal Fibroblasts from Individuals with *CSPP1*-Related JBTS

(A) CSPP1 localized to the centrioles in dermal fibroblasts from individuals with *CSPP1*-related JBTS (UW097-3 and UW141-3) and controls. Fibroblasts were immunostained with anti-CSPP1 (red) and antibodies to the basal body marker γ-tubulin (green). The arrowheads point at the colocalization of both proteins. The arrow marks the localization of CSPP1 in the ciliary axoneme only in control cells. DNA was visualized with Hoechst 33258 (blue). Scale bars represent 2 μm.

(B) CSPP1 signal was absent from the axoneme of the primary cilium but remained at the basal body in affected fibroblasts. Serum-starved affected and control fibroblasts were immunostained with anti-CSPP1 (red) and antibodies to the ciliary axoneme marker acetylated α-tubulin (green). The arrowheads mark the location of acetylated-α-tubulin-positive cilia. Note the absence of CSPP1 in the ciliary axoneme of affected fibroblasts. DNA was visualized with Hoechst 33258 (blue). Scale bars represent 5 μm.

JBTS-associated gene function has been shown to result in reduced axonemal localization of ciliary proteins, such as ARL13B and AC3,[26,31] and that our results show that *cspp1* knockdown in zebrafish leads to decreased ciliary localization of Arl13b, we examined the levels of ARL13B and AC3 in primary cilia of control and UW097-3 (with normal numbers of primary cilia) cell lines by measuring raw integrated fluorescence intensity divided by ciliary area. Although most cilia were positive for ARL13B in the UW097-3 cell line (Figures 4D and 4E), we found that the amount of axonemal ARL13B was 20% less than that of the control ($p < 0.0001$; Figures 4D and 4F). A similar effect was seen in the UW141-3 cell line, which had fewer cilia (Figure 4D).

AC3 localized to the primary cilium at similar percentages in both control and UW097-3 cell lines (Figures 5A and 5B). However, in the UW141-3 cell line, only 39% of the remaining cilia were AC3 positive (Figures 5A and 5B). Furthermore, in the UW097-3 cell line, the amount of AC3 signal in the axoneme was 48% lower than that in the control ($p < 0.0001$; Figures 5A and 5C).

Discussion

We have shown that loss of *CSPP1* function causes ~5% of JBTS in humans and results in ciliopathy phenotypes in zebrafish. The spectrum of *CSPP1*-related human phenotypes is broad, including two brothers with typical clinical features of JBTS (hypotonia, ataxia, oculomotor apraxia, and mild cognitive dysfunction), but only a subset of the characteristic imaging features. Moreover, mutations in *CSPP1* are a major cause of the previously reported co-occurrence of JBTS and JATD,[14] explaining three of the six families affected by this phenotype in our cohort. On the basis of the currently available human data, *CSPP1* mutations are not highly associated with retinal, kidney, or liver involvement in humans, although these features do occur. Similar to loss of *CSPP1* function in humans, loss of *cspp1* function in zebrafish affects skeletal development and results in pronephric cysts (analogous to human cystic kidney disease). Lastly, loss of CSPP1 function in humans appears to affect primary cilium

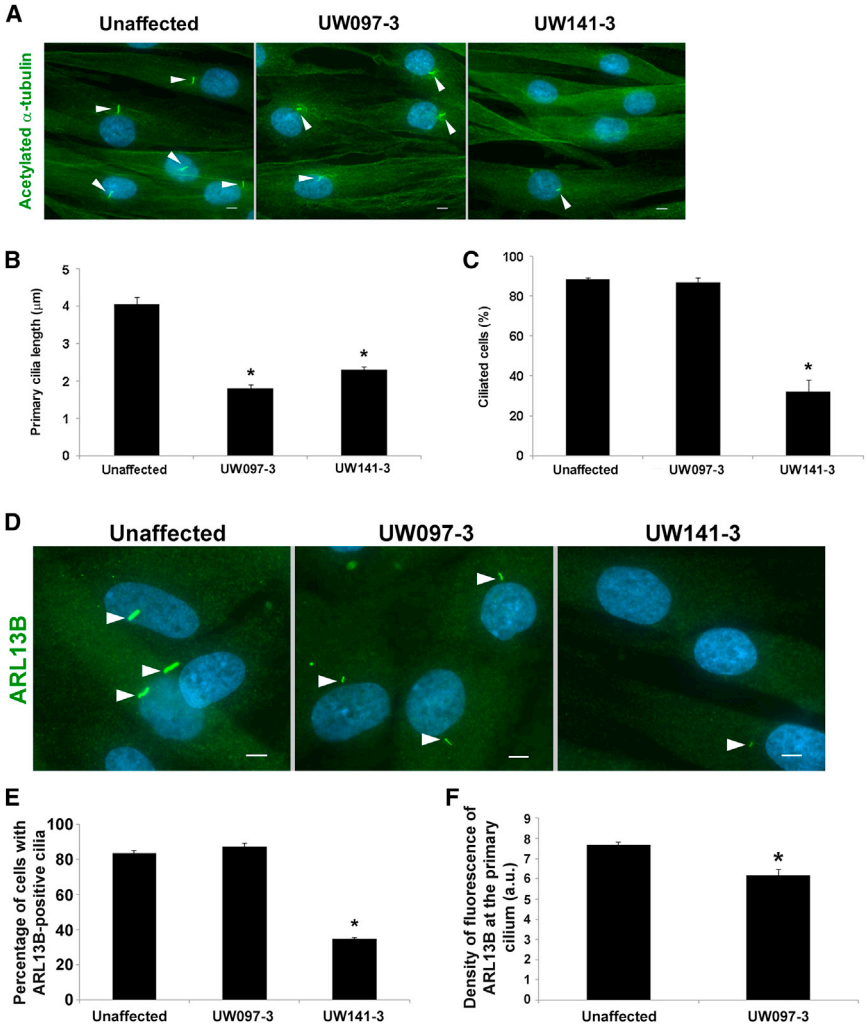

Figure 4. Dermal Fibroblasts from Individuals with *CSPP1*-Related JBTS Mutations Have Short Cilia and Abnormal Ciliary ARL13B Localization

(A) Primary cilia on affected and control fibroblasts immunostained for acetylated α-tubulin. Arrowheads point to primary cilia. DNA was stained with Hoechst 33258 (blue). Scale bars represent 5 μm.

(B) Fibroblasts from individuals with *CSPP1*-related JBTS had shorter primary cilia. Dermal fibroblasts were immunostained with anti-acetylated α-tubulin, and cilia lengths were measured with AxioVision software. Results are expressed as the mean ± SEM. *$p < 0.0001$.

(C) UW141-3 fibroblasts had fewer cilia. For quantifying cilia, the number of cells with acetylated-α-tubulin positive cilia were counted (>100 cells per coverslip). Results are expressed as the mean ± SEM ($n = 3$). *$p < 0.01$.

(D) Fibroblast cell lines immunostained with anti-ARL13B and Hoechst 33258. Arrowheads point at primary cilia. Scale bars represent 5 μm.

(E) ARL13B localized to the primary cilium in unaffected and affected fibroblasts; the UW141-3 cell line had fewer ARL13B-positive cilia. The number of cells with ARL13B immunolabeling at primary cilia was counted in 300 cells per cell line. Results are expressed as the mean ± SEM. *$p < 0.001$.

(F) The ciliary distribution of ARL13B was reduced in affected fibroblasts. Images of ARL13B immunolabeling in control and affected cells were taken with the same settings, and fluorescence density of ARL13B immunostaining at the primary cilium was quantified in >20 cells with ImageJ. Results are expressed as the mean ± SEM. *$p < 0.0001$.

formation, length, and trafficking of ciliary proteins to the axoneme.

The decreased cilium number and length in cell lines with *CSPP1* mutations are similar to the effects seen with loss-of-function mutations in several other genes involved in JBTS.[32,33] In addition, prior work has shown that CSPP1 overexpression in hTERT-RPE cells results in longer cilia.[25] These observations, in combination with our own, suggest that CSPP1 might be involved in the control of cilia length. Although it is not possible to draw a genotype-phenotype conclusion on the basis of two cell lines, the cell line with the more N-terminal truncating mutations (UW141-3) has both reduced cilium number and length, whereas the line with more C-terminal truncating mutations (UW097-3) only has reduced cilium length.

The majority of proteins involved in the pathogenesis of JBTS localize to the basal body or transition zone of the primary cilium, where they form functional complexes. The transition zone controls the transport of proteins such as AC3 and ARL13B in and out of the primary cilium[28,34] through the tectonic and NPHP complexes.[26,30] Similarly, we have shown that CSPP1 is required for localization of AC3 and ARL13B to the primary cilium. Patzke et al. demonstrated that CSPP1 binds RPGRIP1L (NPHP8) and NPHP4 in a complex,[25] providing additional evidence that CSPP1 functions at the transition zone. However, CSPP1 also localizes to the ciliary axoneme, so it could function there as well.

In conclusion, our results demonstrate that mutations in *CSPP1* cause JBTS, including the JBTS-JATD ciliopathy phenotype. Although CSPP1 is required for localization of axonemal proteins, such as ARL13B and AC3, how loss of CSPP1 function leads to both JBTS and JATD remains unknown. Given the prominent role of intraflagellar transport (IFT) in the mechanisms underlying JATD, CSPP1 might participate in the IFT-dependent localization of axonemal proteins required for skeletal development. Future work will focus on identifying additional components of the functional networks underlying JBTS and JATD, as well as understanding how genetic perturbations result in the broad spectrum of phenotypes seen in individuals with JBTS.

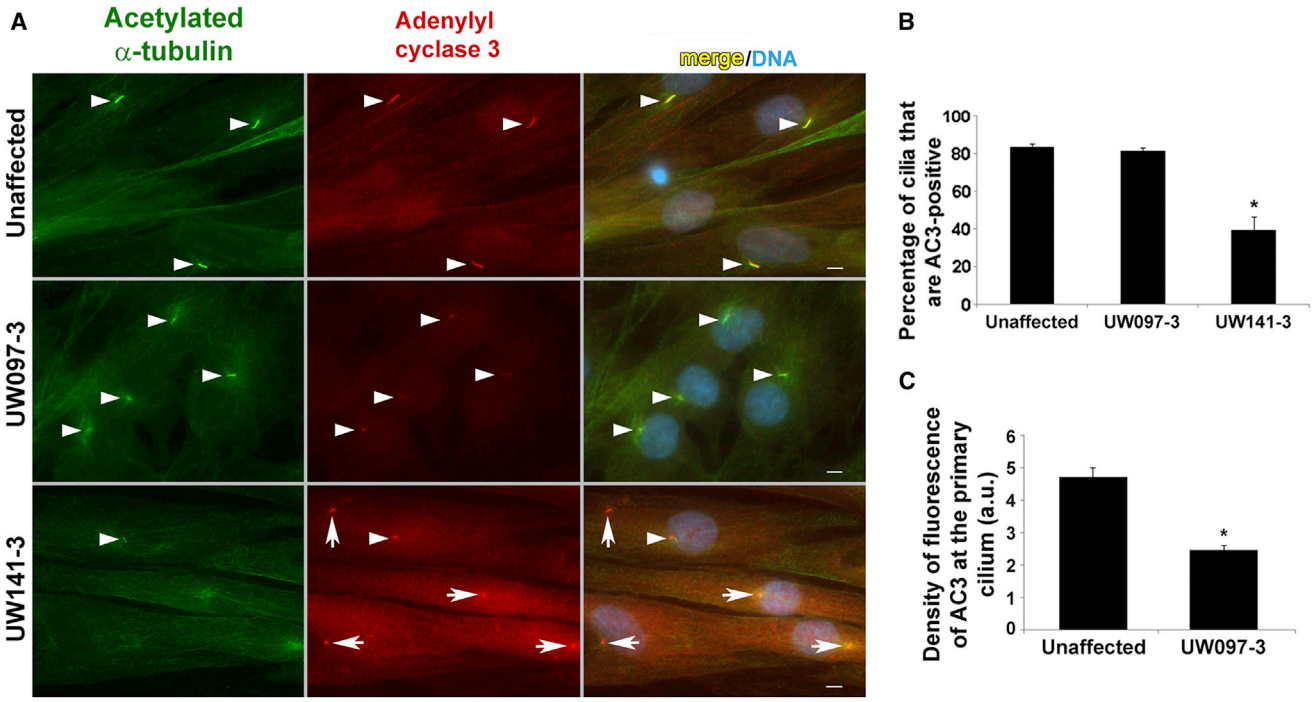

Figure 5. AC3 Localization to Primary Cilia Is Reduced in Fibroblasts from Individuals with *CSPP1*-Related JBTS
(A) Acetylated α-tubulin and AC3 immunostaining. Arrowheads point to primary cilia. Arrows point at the basal body immunolabeled with AC3. DNA was stained with Hoechst 33258 (blue). Scale bars represent 5 μm.
(B) The localization of the ciliary protein AC3 at the remaining primary cilia in JBTS fibroblasts with *CSPP1* mutations was reduced. The number of cells with primary cilia with both acetylated α-tubulin and AC3 were counted in unaffected and JBTS fibroblasts (>300 cells per case). Results are expressed as the mean ± SEM. *$p < 0.05$.
(C) The ciliary distribution of AC3 was diminished in UW097-3 fibroblasts. Images of AC3 immunolabeling in control and affected cells were taken with the same settings, and fluorescence density of AC3 immunostaining at the primary cilium was quantified in >40 cells per genotype with ImageJ. Results are expressed as the mean ± SEM. *$p < 0.0001$.

Supplemental Data

Supplemental Data include four figures and two tables and can be found with this article online at http://www.cell.com/AJHG.

Acknowledgments

Our deepest thanks go to all of the individuals with Joubert syndrome and their families. This work was supported in part by the Swiss National Science Foundation (PZ00P3_142404 to R.B.-G.), the March of Dimes Foundation (5-FY09-29 to R.J.F.), and the National Institute of Neurological Disorders and Stroke of the National Institutes of Health (R01NS064077 and University of Washington Intellectual and Developmental Disabilities Research Center Genetics Core P30HD002274 to D.D. and R01NS064283 to R.J.F.). We also acknowledge private donations from the families of children with Joubert syndrome.

Received: September 2, 2013
Accepted: November 13, 2013
Published: December 19, 2013

Web Resources

The URLs for data presented herein are as follows:

GATK, http://www.broadinstitute.org/gatk/
NHLBI Exome Sequencing Project (ESP) Exome Variant Server, http://evs.gs.washington.edu/EVS/
Online Mendelian Inheritance in Man (OMIM), http://www.omim.org/
Picard, http://picard.sourceforge.net/
SeattleSeq Annotation 137, http://snp.gs.washington.edu/SeattleSeqAnnotation137/

References

1. Brancati, F., Dallapiccola, B., and Valente, E.M. (2010). Joubert Syndrome and related disorders. Orphanet J. Rare Dis. *5*, 20.
2. Doherty, D. (2009). Joubert syndrome: insights into brain development, cilium biology, and complex disease. Semin. Pediatr. Neurol. *16*, 143–154.
3. Sattar, S., and Gleeson, J.G. (2011). The ciliopathies in neuronal development: a clinical approach to investigation of Joubert syndrome and Joubert syndrome-related disorders. Dev. Med. Child Neurol. *53*, 793–798.
4. Poretti, A., Huisman, T.A., Scheer, I., and Boltshauser, E. (2011). Joubert syndrome and related disorders: spectrum of neuroimaging findings in 75 patients. AJNR Am. J. Neuroradiol. *32*, 1459–1463.
5. Hildebrandt, F., Benzing, T., and Katsanis, N. (2011). Ciliopathies. N. Engl. J. Med. *364*, 1533–1543.
6. Jeune, M., Beraud, C., and Carron, R. (1955). [Asphyxiating thoracic dystrophy with familial characteristics]. Arch. Fr. Pediatr. *12*, 886–891.
7. Beales, P.L., Bland, E., Tobin, J.L., Bacchelli, C., Tuysuz, B., Hill, J., Rix, S., Pearson, C.G., Kai, M., Hartley, J., et al. (2007).

IFT80, which encodes a conserved intraflagellar transport protein, is mutated in Jeune asphyxiating thoracic dystrophy. Nat. Genet. *39*, 727–729.

8. Bredrup, C., Saunier, S., Oud, M.M., Fiskerstrand, T., Hoischen, A., Brackman, D., Leh, S.M., Midtbø, M., Filhol, E., Bole-Feysot, C., et al. (2011). Ciliopathies with skeletal anomalies and renal insufficiency due to mutations in the IFT-A gene WDR19. Am. J. Hum. Genet. *89*, 634–643.
9. Dagoneau, N., Goulet, M., Geneviève, D., Sznajer, Y., Martinovic, J., Smithson, S., Huber, C., Baujat, G., Flori, E., Tecco, L., et al. (2009). DYNC2H1 mutations cause asphyxiating thoracic dystrophy and short rib-polydactyly syndrome, type III. Am. J. Hum. Genet. *84*, 706–711.
10. Davis, E.E., Zhang, Q., Liu, Q., Diplas, B.H., Davey, L.M., Hartley, J., Stoetzel, C., Szymanska, K., Ramaswami, G., Logan, C.V., et al.; NISC Comparative Sequencing Program (2011). TTC21B contributes both causal and modifying alleles across the ciliopathy spectrum. Nat. Genet. *43*, 189–196.
11. Keppler-Noreuil, K.M., Adam, M.P., Welch, J., Muilenburg, A., and Willing, M.C. (2011). Clinical insights gained from eight new cases and review of reported cases with Jeune syndrome (asphyxiating thoracic dystrophy). Am. J. Med. Genet. A. *155A*, 1021–1032.
12. Oberklaid, F., Danks, D.M., Mayne, V., and Campbell, P. (1977). Asphyxiating thoracic dysplasia. Clinical, radiological, and pathological information on 10 patients. Arch. Dis. Child. *52*, 758–765.
13. McInerney-Leo, A.M., Schmidts, M., Cortés, C.R., Leo, P.J., Gener, B., Courtney, A.D., Gardiner, B., Harris, J.A., Lu, Y., Marshall, M., et al.; UK10K Consortium (2013). Short-rib polydactyly and Jeune syndromes are caused by mutations in WDR60. Am. J. Hum. Genet. *93*, 515–523.
14. Lehman, A.M., Eydoux, P., Doherty, D., Glass, I.A., Chitayat, D., Chung, B.Y., Langlois, S., Yong, S.L., Lowry, R.B., Hildebrandt, F., and Trnka, P. (2010). Co-occurrence of Joubert syndrome and Jeune asphyxiating thoracic dystrophy. Am. J. Med. Genet. A. *152A*, 1411–1419.
15. O'Roak, B.J., Vives, L., Fu, W., Egertson, J.D., Stanaway, I.B., Phelps, I.G., Carvill, G., Kumar, A., Lee, C., Ankenman, K., et al. (2012). Multiplex targeted sequencing identifies recurrently mutated genes in autism spectrum disorders. Science *338*, 1619–1622.
16. Li, H., and Durbin, R. (2010). Fast and accurate long-read alignment with Burrows-Wheeler transform. Bioinformatics *26*, 589–595.
17. DePristo, M.A., Banks, E., Poplin, R., Garimella, K.V., Maguire, J.R., Hartl, C., Philippakis, A.A., del Angel, G., Rivas, M.A., Hanna, M., et al. (2011). A framework for variation discovery and genotyping using next-generation DNA sequencing data. Nat. Genet. *43*, 491–498.
18. Westerfield, M. (2000). The zebrafish book. A guide for the laboratory use of zebrafish (Danio rerio) (Eugene: University of Oregon Press).
19. Sun, Z., Amsterdam, A., Pazour, G.J., Cole, D.G., Miller, M.S., and Hopkins, N. (2004). A genetic screen in zebrafish identifies cilia genes as a principal cause of cystic kidney. Development *131*, 4085–4093.
20. Schneider, C.A., Rasband, W.S., and Eliceiri, K.W. (2012). NIH Image to ImageJ: 25 years of image analysis. Nat. Methods *9*, 671–675.
21. Javidan, Y., and Schilling, T.F. (2004). Development of cartilage and bone. Methods Cell Biol. *76*, 415–436.
22. Pathak, N., Obara, T., Mangos, S., Liu, Y., and Drummond, I.A. (2007). The zebrafish fleer gene encodes an essential regulator of cilia tubulin polyglutamylation. Mol. Biol. Cell *18*, 4353–4364.
23. Sukumaran, S., and Perkins, B.D. (2009). Early defects in photoreceptor outer segment morphogenesis in zebrafish ift57, ift88 and ift172 Intraflagellar Transport mutants. Vision Res. *49*, 479–489.
24. Eberhart, J.K., Swartz, M.E., Crump, J.G., and Kimmel, C.B. (2006). Early Hedgehog signaling from neural to oral epithelium organizes anterior craniofacial development. Development *133*, 1069–1077.
25. Patzke, S., Redick, S., Warsame, A., Murga-Zamalloa, C.A., Khanna, H., Doxsey, S., and Stokke, T. (2010). CSPP is a ciliary protein interacting with Nephrocystin 8 and required for cilia formation. Mol. Biol. Cell *21*, 2555–2567.
26. Garcia-Gonzalo, F.R., Corbit, K.C., Sirerol-Piquer, M.S., Ramaswami, G., Otto, E.A., Noriega, T.R., Seol, A.D., Robinson, J.F., Bennett, C.L., Josifova, D.J., et al. (2011). A transition zone complex regulates mammalian ciliogenesis and ciliary membrane composition. Nat. Genet. *43*, 776–784.
27. Hsiao, Y.C., Tong, Z.J., Westfall, J.E., Ault, J.G., Page-McCaw, P.S., and Ferland, R.J. (2009). Ahi1, whose human ortholog is mutated in Joubert syndrome, is required for Rab8a localization, ciliogenesis and vesicle trafficking. Hum. Mol. Genet. *18*, 3926–3941.
28. Hsiao, Y.C., Tuz, K., and Ferland, R.J. (2012). Trafficking in and to the primary cilium. Cilia *1*, 4.
29. Huang, L., Szymanska, K., Jensen, V.L., Janecke, A.R., Innes, A.M., Davis, E.E., Frosk, P., Li, C., Willer, J.R., Chodirker, B.N., et al. (2011). TMEM237 is mutated in individuals with a Joubert syndrome related disorder and expands the role of the TMEM family at the ciliary transition zone. Am. J. Hum. Genet. *89*, 713–730.
30. Sang, L., Miller, J.J., Corbit, K.C., Giles, R.H., Brauer, M.J., Otto, E.A., Baye, L.M., Wen, X., Scales, S.J., Kwong, M., et al. (2011). Mapping the NPHP-JBTS-MKS protein network reveals ciliopathy disease genes and pathways. Cell *145*, 513–528.
31. Tuz, K., Hsiao, Y.C., Juárez, O., Shi, B., Harmon, E.Y., Phelps, I.G., Lennartz, M.R., Glass, I.A., Doherty, D., and Ferland, R.J. (2013). The Joubert syndrome-associated missense mutation (V443D) in the Abelson-helper integration site 1 (AHI1) protein alters its localization and protein-protein interactions. J. Biol. Chem. *288*, 13676–13694.
32. Larkins, C.E., Aviles, G.D., East, M.P., Kahn, R.A., and Caspary, T. (2011). Arl13b regulates ciliogenesis and the dynamic localization of Shh signaling proteins. Mol. Biol. Cell *22*, 4694–4703.
33. Lee, J.E., Silhavy, J.L., Zaki, M.S., Schroth, J., Bielas, S.L., Marsh, S.E., Olvera, J., Brancati, F., Iannicelli, M., Ikegami, K., et al. (2012). CEP41 is mutated in Joubert syndrome and is required for tubulin glutamylation at the cilium. Nat. Genet. *44*, 193–199.
34. Craige, B., Tsao, C.C., Diener, D.R., Hou, Y., Lechtreck, K.F., Rosenbaum, J.L., and Witman, G.B. (2010). CEP290 tethers flagellar transition zone microtubules to the membrane and regulates flagellar protein content. J. Cell Biol. *190*, 927–940.